Effects of divalent salts on polyelectrolyte coacervation

Jacob D. Horne,[†,¶] Kayla Patricia Barker,[‡,¶] Yan Xia,[*,‡] and Jian Qin[*,†]

†*Department of Chemical Engineering, Stanford University, Stanford, California 94305, USA*

‡*Department of Chemistry, Stanford University, Stanford, California 94305, USA*

¶*Contributed equally to this work*

E-mail: yanx@stanford.edu; jianq@stanford.edu

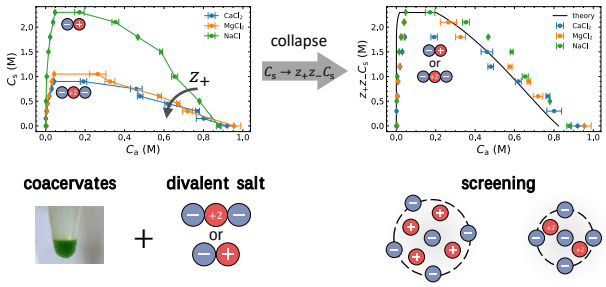

for table of contents use only

Abstract

Polyelectrolyte solutions exhibit a demixing transition known as polyelectrolyte complexation (PEC). Recent interest in PEC has been spurred by its relevance in organizing biomolecules in intracellular environments, and by the advancement of theoretical treatments. A range of molecular parameters has been shown to influence the demixing transition, including charge patterning, polarity, stoichiometry, etc. We

present a study on the effects of ion valency, which remains largely unexplored. We leverage our previous expertise in synthesizing homologous polyelectrolytes to investigate how the addition of divalent ions (Ca^{2+}, Mg^{2+}) affects their complexation behavior and ion partitioning. Dye-labeled polyelectrolytes and ICP-MS measurements enable the construction of accurate complexation phase diagrams as well as quantification of ion partitioning. The two-phase window is found to be substantially narrower than the case of monovalent ions, while the ion and polymer partitioning are similar to those for monovalent ions. The results are rationalized by analyzing how ion valency reduces the ionic correlations, which enables the collapse of phase diagrams for both monovalent and divalent ions.

1 Introduction

Polyelectrolyte solutions exhibit a demixing transition known as polyelectrolyte complexation (PEC), owing to the electrostatic interactions among the charged groups.[1–3] PEC results in the coexistence between a supernatant that is nearly depleted of polymers, and a polymer-rich complex.[1–3] The complex may behave as a solid-like precipitate, or flow and coalesce like a liquid.[1–3] Such liquid-like complexes are often referred to as coacervates, and the demixing transition as coacervation.[1–3]

Renewed interest in PEC has been spurred by its recognition as an important mechanism in organizing biomolecules in intracellular environments,[4,5] and by the advancement of theoretical treatments of PEC.[2,3,6] Recent works have successfully incorporated the effects of polyelectrolyte backbone polarity,[2,7,8] chain structure or conformation,[9] reversible charge regulation or ion-binding reactions,[8,10,11] charge patterning,[12] and adaptive chain structure factors[13,14] into theoretical descriptions of PEC. Such works have enabled substantial improvements in describing the behavior of the complex phase. Likewise, recent theoretical[15] and computational[16] work has advanced the understanding and description of the supernatant phase. From an experimental perspective, many recent studies have devel-

oped well-defined systems that enabled detailed investigation of the effects of key molecular features on coacervate phase behavior; for example, polyelectrolyte chain length,[17,18] backbone polarity,[8] solvent quality,[19] temperature,[20,21] and polyelectrolyte stoichiometry[22] have been investigated.

These studies have been thoroughly discussed in recent reviews.[1–3,7] For the current work, it is relevant to note that stoichiometric mixtures of homologous linear polyanions, polycations, and their counterions (endogenous salt) are known to readily undergo PEC when the backbone charge density or electrostatic strength is sufficiently large. This phase separation persists under small amounts of added (exogenous) salt until some critical salt concentration, $C_{\mathrm{s}}^{\mathrm{ct.}}$, is reached. Above this exogenous salt concentration the mixture no longer undergoes PEC, owing to the decreased magnitude of electrostatic interactions due to charge screening at high ionic strengths. The value of $C_{\mathrm{s}}^{\mathrm{ct.}}$ is highly dependent on the chemistry of the polyion, counterions, exogenous salt, and solvent: it is higher for polyions with larger degrees of polymerization,[8] larger backbone charge densities,[23] smaller persistence lengths,[14] and lower compatibility with the solvent.[8,19]

Most of these works considered monovalent ions. Multivalent ions, e.g. Ca^{2+} and Mg^{2+}, are commonly found in both biological and synthetic systems, and their presence may induce condensation or collapse of charged biopolymers such as DNA.[24,25] The properties of condensed polyelectrolytes change substantially when the valence of the added salt is altered.[26] For instance, the formation of gel phases,[27] which can manifest as disease states in biological systems,[28] is related to the presence of high-valence salts. The abundant experimental[24,29–33] and theoretical[24,30,33–36] studies on polyelectrolyte precipitation in the presence of multivalent ions suggest that, the intra- and inter-chain electrostatic interactions, either screened or mediated by multivalent ions, are both important.

Along this line, there is a consensus regarding the conditions causing precipitation of polyelectrolytes when trivalent or tetravalent salts, e.g. $LaCl_3$ or $Th(NO_3)_4$, are introduced. In these cases, precipitation occurs in a range of salt concentrations $C_{\mathrm{s}}^{*} \leq C_{\mathrm{s}} \leq C_{\mathrm{s}}^{**}$, outside

which the solution is homogeneous.[29,30,32] The lower bound C_s^* has been attributed to favorable interactions between multivalent ions and oppositely charged monomers and increases nearly linearly with the polymer concentration. The upper (re-entrant) bound C_s^{**} is often attributed to weakened electrostatic interactions due to ion screening, and is found to be nearly independent of polymer concentration.

To rationalize these observations, counterion condensation and the bridging effects caused by the multivalent cations that are simultaneously bound to different polyanions were considered.[29] The free energy of condensation and bridging was estimated. The calculated spinodal line was shown to agree qualitatively with experimental data. An alternative work[36] considers composition fluctuations without explicitly accounting for the bridging effects. Binodal curves were calculated, which also agrees with the trend mentioned above.

For divalent ions, such as $BaCl_2$ or $CaCl_2$, a variety of behaviors have been reported.[32] In some cases, the lower bound C_s^* has been found to increase nonlinearly with polymer concentration,[37] consistent with the requirement of the law of mass action. In other cases,[32,38,39] it was found to remain constant or even decrease with increasing polymer concentration. The re-entrant bound C_s^{**} was reported in some cases,[30,32,40] but is missing in other cases even up to a high salinity, $C_s \approx 1\,\text{M}$.[32] Furthermore, light[32] and neutron[32] scattering analysis of these solutions indicates the presence of spherical or cylindrical polymer domains (about 10 nm) in the presence of divalent ions, which are not observed for other ion valences. The origin to such specific effects is unknown.

Beyond these studies, little is known of the effects of ion valence on polyelectrolyte complexation. The preliminary efforts[41] conclude that, by monitoring the turbidity of solutions with fixed composition, high-valence salt suppresses the coacervation window more strongly than low-valence salt. While valence was found to be the primary factor affecting salt stability, small differences were observed between different ions of the same valence, for instance $CaCl_2$ and $MgCl_2$, which was attributed to the Hofmeister effects.[41–44]

Few works have constructed phase diagrams. A recent theoretical study[45] shows that in-

creasing valence suppresses the two-phase window and that the divalent ions, similar to the monovalent ions,[2,18,22,46,47] are enriched in the supernatant phase. In contrast, an experimental study[48] determined the binodal phase diagram using thermal degradation measurements. The effects of NaCl, $CaCl_2$, and $SrCl_2$ salts were compared. No strong salt resistance was reported, and divalent ions were found to be enriched in the coacervate phase.

To partially resolve the above discrepancy, in this work, we studied the effect of salt valence on coacervation. As in our previous studies,[8,22] we used homologous polyelectrolytes, i.e. polycations and polyanions with identical backbones as a model system and generated binodal phase diagrams when either monovalent or divalent ions were added. The concentrations of polymers in both the supernatant and coacervate phases were determined from the absorbance of dye-labeled polyelectrolytes, and those of ions were determined using inductively coupled plasma mass spectrometry (ICP-MS). A direct comparison of phase diagrams and salt partitioning was then made between the monovalent and divalent cases. A substantial suppression of two phase window was found for the divalent case. The results were analyzed and rationalized using the model we developed earlier,[8,11,22] generalized to account for the effects of ion valency.

2 Experimental and theoretical methods

2.1 Polyelectrolyte synthesis and dye-labeling

Polacrylamide-based polyanions and polycations of length $N = 50$ were synthesized using the same precursor polymer made by reversible addition-fragmentation transfer (RAFT) polymerization and a series of postpolymerization modifications, detailed in our previous works.[8,22]

Sulfo-Cy5 amine was conjugated to the end group of the polyanion via carbodiimide coupling (at 1 Sulfo-Cy5 per 24 polymer chains) according to our previously reported procedure.[22] Polyanion concentrations were determined by absorbance measurements at 649 nm.

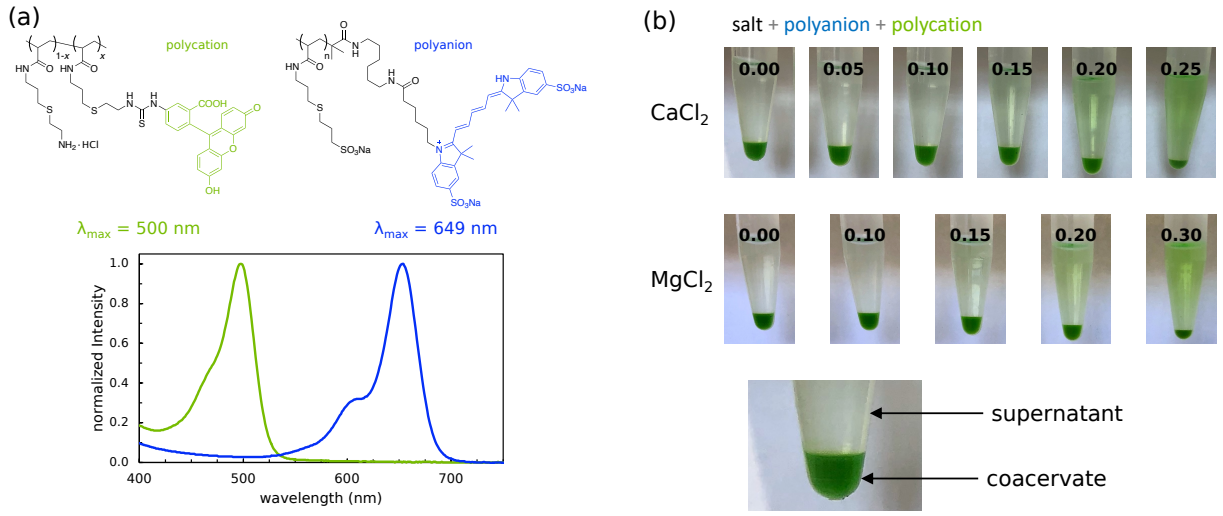

Figure 1: (a) Chemical structures of dye-labeled polycations and polyanions, and the UV absorption spectra of these PEs. (b) Photographs of phase separation upon mixing of oppositely charged PEs and divalent salts. Molar concentrations of added salt are labeled on each sample tube.

Fluorescein isothiocyanate (FITC) was conjugated to the amine groups on the polycation. Polycation (890.3 mg) was dissolved in 1× PBS buffer (*p*H 7.4, 9.35 mL). FITC (0.997 mg, 0.0006 equiv per amine) was added to the polymer solution as a stock solution in 1× PBS (0.4 mg/mL) and stirred overnight at room temperature. The reaction mixture was dialyzed against NaCl (4 g/L) for 1.5 days, against deionized H_2O for 1.5 days, and lyophilized for 3 days to obtain a light yellow powder (1 FITC per 32 polymer chains). Polycation concentrations were measured by absorbance at 494 nm.

2.2 Measurement of experimental binodal diagrams

Individual stock solutions of polycations and polyanions in Milli-Q water were prepared at a concentration of 8 wt%. The *p*H of the stock solutions were adjusted to *p*H 7.4 using 1 M NaOH. The polyelectrolyte stock solutions were mixed at 1:1 stoichiometry with a total polymer concentration of 100 mM. Varying amounts of NaCl, $CaCl_2$, and $MgCl_2$ were added to 1:1 polyelectrolyte mixtures and they were equilibrated at room temperature for 2 days before measurement of polymer concentrations. The supernatant and coacervate

phases were separated and their volumes were determined using a calibrated pipette. The supernatants were diluted before ultraviolet-visible (UV-vis) absorbance measurements. The coacervate phase was lyophilized and redissolved in 1 mL of PBS buffer containing 2 M NaCl, followed by dilution before UV-vis absorbance measurements. Polyelectrolyte concentrations were determined using calibration curves from the labelled polymers (**Fig. S.1**). Polyanion concentrations were used for construction of binodal curves.

Na^+, Ca^{2+}, and Mg^{2+} concentrations were measured using ICP-MS. Cl^- values are difficult to measure at these low concentrations using ICP-MS and are not included in our analysis. Standard curves were constructed by dissolving known amounts of NaCl, $CaCl_2$, and $MgCl_2$ in deionized water containing 0.5 mM KOH. KOH is added to the samples to prevent coacervation after dilution of superntant and coacervate samples. $CaCl_2$ and $MgCl_2$ are both soluble at low concentrations in the water and 0.5 mM KOH matrix. Supernatant samples were directly diluted in the same matrix. Coacervates were lyophilized and redissolved in 200 µL 1 mol dm^{-3} KBr solution before dilution. Error bars, where shown, are obtained from measurements completed in triplicate.

2.3 Theory

The model used to analyze the experimental data is based on our previous work,[8,11,22] generalized for multi-valent ions. We consider a system with total volume V, polyelectrolyte volume fraction $\phi_{\rm p}$, and salt volume fraction $\phi_{\rm s}$. The polyanions and polycations are identical except for the sign of charge. Every monomer carries either $+1$ or -1 charge. Each polyion contains N monomers, and their volume fractions are $\phi_{\rm a}$ and $\phi_{\rm c}$. The small cations and anions have volume fractions ϕ_+ and ϕ_-, which relate to the total salt volume fraction by $\phi_{\rm s} = \phi_+ + \phi_-$. For simplicity, their volumes are assumed equal, and their valences are denoted $+z_+$ and $-z_-$. Charge neutrality requires that, for the exogenous salts, $\phi_+ z_+ = \phi_- z_-$ and $\phi_\pm = \phi_{\rm s}\, z_\mp/(z_+ + z_-)$.

To facilitate unit conversion, a single reference volume is used for monomers and small

ions, and is set to the volume of a water molecule, $v_0 = 30\,\text{Å}^3$. The species volumes, v_i (i = p, and s), are normalized as $\omega_i = v_i/v_0$. Note that ω_p is the normalized volume of a polyion *monomer* rather than the entire chain. A common length, $l_0 = v_0^{1/3}$, is also used for nondimensionalization.

Following our earlier treatment, the dimensionless free energy is expressed as a sum of three contributions,

$$f = \frac{F v_0}{k_\text{B} T V} = f_\text{m} + f_\chi + f_\text{e}. \tag{1}$$

The first term has the standard form, which captures the translational entropy of solvent, polyelectrolytes, and dissolved ions,

$$f_\text{m} = \phi_\text{W} \ln \phi_\text{W} + \frac{1}{N\omega_\text{p}}(\phi_\text{a} \ln \phi_\text{a} + \phi_\text{c} \ln \phi_\text{c}) + \frac{1}{\omega_\text{S}}(\phi_+ \ln \phi_+ + \phi_- \ln \phi_-). \tag{2}$$

The volume fraction of solvent ϕ_W is computed from $\phi_\text{W} = 1 - \phi_\text{a} - \phi_\text{c} - \phi_+ - \phi_-$ by imposing the incompressibility condition.

The second term captures the short-range dispersion interactions between polymers and solvent via the Flory-Huggins parameter χ,

$$f_\chi = \chi\, \phi_\text{W}(\phi_\text{a} + \phi_\text{c}). \tag{3}$$

Because polyanions and polycations have identical backbones, a single χ parameter suffices, and no additional term is needed to account for polymer-polymer interactions. In our analysis, the value of χ is tuned to fit experimental data.

The third term captures the contribution from Coulombic interactions. For homogeneous supernatant or coacervate phases, the bulk charge density vanishes because of charge neutrality. The non-vanishing contributions to Coulombic energy have to arise from composition fluctuations. For weak composition fluctuations, the free energy can be described by the

random phase approximation (RPA),[2,9,49,50]

$$f_{\mathrm{e}} = \frac{1}{4\pi^2}\int_0^\infty \mathrm{d}q\, q^2 \ln\left(1+\frac{\kappa^2(q)}{q^2}\right), \tag{4}$$

$$\kappa^2(q) \equiv 4\pi l_{\mathrm{B}}\Big[z_+^2\,\tilde{\Omega}_+(q) + z_-^2\,\tilde{\Omega}_-(q) + \sigma^2\Big(\tilde{\Omega}_{\mathrm{A}}(q)+\tilde{\Omega}_{\mathrm{C}}(q)\Big)\Big]. \tag{5}$$

This formulation of the electrostatic correlation free energy is a result of Gaussian treatment on charge density fluctuation, and has been extensively discussed previously.[2,9,11,14,49,50] While relegating detailed derivations and discussion to literature, we note that the RPA tends to overestimate the stability of the coacervate in the high-salt regime. Therefore, our analysis below, section 3.3, is focused on the the low-salt regime.

The integration in eq. (4) is over the wavenumber q, non-dimensionalized by l_0. The term $\kappa^{-1}(q)$ is the q-dependent screening length. It measures how effectively the Coulombic interaction is screened by small ions and charges on polymers, and is analogous to the Debye length.[51,52] The strength of the Coulombic interaction is quantified by the dimensionless Bjerrum length, $l_{\mathrm{B}} \equiv \mathrm{e}^2/(4\pi\epsilon k_{\mathrm{B}}T l_0)$, in which e is the elementary charge, and ϵ is the static dielectric permittivity. The expression implicitly assumes that the dielectric medium can be adequately treated by the bulk value of static permittivity. The effects of the discrete solvation structure has been considered recently.[53,54] Here, to focus on the effects of ion valence, we still adopt the continuum treatment. For an aqueous solution at room temperature, we have $l_{\mathrm{B}} \approx 2.29$.

In eq. (5), σ is the fraction of charged monomers on each polycation and polyanion; each chain thus has a total charge of $\pm\sigma N$. The terms $\tilde{\Omega}_i(q)$ are the intramolecular correlation functions for small ions and polyanions given, respectively, by

$$\tilde{\Omega}_{\pm}(q) = \frac{\phi_{\pm}}{\omega_{\mathrm{S}}}\,\hat{\Gamma}_{\mathrm{s}}^2(q), \tag{6}$$

$$\tilde{\Omega}_{\mathrm{A/C}}(q) = \frac{\phi_{\mathrm{A/C}}}{\omega_{\mathrm{p}}} N g(q)\,\hat{\Gamma}_{\mathrm{p}}^2(q). \tag{7}$$

The q-dependence in eq. (6) for the small ions derives from that of the factors, $\hat{\Gamma}_i(q) \equiv \exp(-q^2 a_i^2/2)$, which effectively smear point-like charges to a Gaussian cloud with finite width a_i. Introducing the smearing functions prevents the high-q divergence of the integral in eq. (4), a well-known pathology resulting from the replacement of Coulombic interactions between point-like ions with those between continuum charge density fields.[9,11] This regularization is unnecessary for systems with a fixed number of dissociated ions, for which the divergence can be removed by redefining the reference state for energy. However, for systems with variable degrees of ion association, it is needed in order to properly evaluate the solvation free energy of both small ions and polyelectrolytes.[11] The factor $\hat{\Gamma}_{\mathrm{p}}^2$ in eq. (7) plays an analagous role to $\hat{\Gamma}_{\mathrm{s}}^2$.

Finally, the term $g(q)$ in eq. (7) is the single chain structure factor, which incorporates the effects of charge connectivity. When the polymer conformation is Gaussian, $g(q)$ is given by the Debye function, $g_{\mathrm{D}}(x) = 2(x - 1 + e^{-x})/x^2$, where $x \equiv q^2 R_{\mathrm{g}}^2$ and $R_{\mathrm{g}}^2 = Nb^2/6$ is the dimensionless mean squared radius of gyration. The analysis in this work at the low-salt regime assumes that chains are Gaussian. The effects of rod-like[9] and adaptive chain structure factors have been discussed in our earlier work.[14]

In summary, the model is essentially based on our earlier work.[8,11,22] By explicitly including salt valences z_+ and z_-, and by analyzing the variation of model predictions, we will show that the experimental trend can be rationalized by the enhanced screening. In particular, the asymptotic analysis in the low-salt regime allows for the collapse of phase diagrams in both monovalent and divalent systems.

3 Results and discussion

3.1 Effect of valence on phase behavior

Polyacrylamides with pendant sulfonate and ammonium groups were synthesized, using our previously reported method,[8,22] with identical chain lengths ($N = 50$) and charge densities.

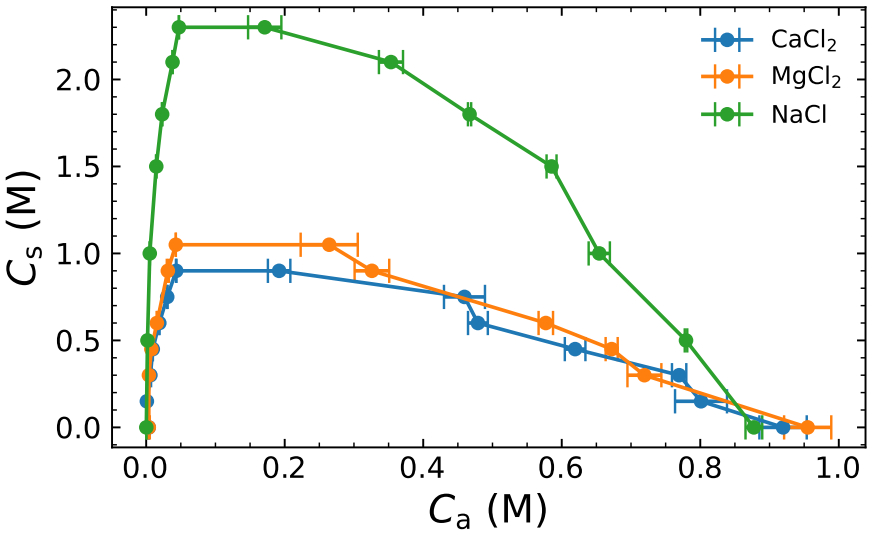

Figure 2: Experimental binodal curves for the polyanion concentration C_a. Vertical axis values correspond to experimentally targeted *bulk exogenous* salt concentrations C_s.

Polyanions and polycations were labeled with two different fluorescent dyes with baseline-separated UV-vis absorbance spectra, allowing for accurate and independent quantification of polyanion and polycation concentrations in coacervate and supernatant phases (**Fig. 1a**). Labeled polyelectrolytes were mixed at a 1:1 ratio with varying amounts of added NaCl, $CaCl_2$, and $MgCl_2$. Because precipitates formed at high salt concentrations with dye-labeled polycations, polycation concentrations cannot be reliably measured at high salt concentrations. Thus, the phase behavior is summarized using polyanion binodal concentrations. The phase diagrams plotted against total polymer concentration are included in the SI (**Fig. S.2**), and the polycation-polyanion stoichiometry is considered in **Sec. 3.2**.

The polyanion binodal curves obtained from UV-vis absorbance measurements are shown in **Fig. 2**, where C_s and C_a are total ion and polyanion concentrations. The three curves are phase diagrams for NaCl, $CaCl_2$, and $MgCl_2$. The C_s axis indicates the *bulk exogenous* total ion concentration. This accounts for the extra chloride ion in the cases of $CaCl_2$ and $MgCl_2$ but does not include the concentration of neutralizing counterions or show coacervate and supernatant salt concentrations.

For both monovalent (NaCl) and divalent ($CaCl_2$, $MgCl_2$) cases, adding salts narrows the

width of the two-phase window, which can be attributed to the weakening of electrostatic correlations due to ionic screening.[3] However, the effects of screening are much stronger in the divalent cases: the maximum total ion concentrations in the binodal curves are 0.9 M for $CaCl_2$ and 1.05 M for $MgCl_2$, as compared to 2.3 M for the monovalent case. The enhanced screening effects of multivalent ions will be analyzed more quantitatively below. These results are in agreement with the existing experimental[41] and theoretical[45] results in the literature, both of which indicate a decrease in salt resistance when the valence of one of the small ions is increased from 1 to 2.

The binodal curves for the two divalent cases, using $CaCl_2$ and $MgCl_2$, are nearly identical. This suggests that the difference in ion-specific effects, such as solvation free energy, is likely small between Ca^{2+} and Mg^{2+}. Further, the agreement between the results from distinct ions implies that the trend may be modeled by focusing on the valence alone, which we shall demonstrate in the following section. Finally, our results appear to be consistent with the turbidity curves for Ca^{2+} and Mg^{2+} in ref. 41. Both turbidity measurements and our binodal diagrams indicate a slightly weaker salt resistance for Ca^{2+} than Mg^{2+}. Such difference was noted previously as a weak Hofmeister effect.[41] Given that the difference is within the range of noise, however, we shall conclude that such Hofmeister effect is negligible in our systems.

Our results can be compared to the literature study[48] that reports binodal diagrams for different pairs of polymers but a similar set of salts (NaCl, $CaCl_2$, $SrCl_2$). Unfortunately, no clear trend in polymer concentration can be discerned for the monovalent case in Fig. 1c of ref. 48, which may be caused by the limited accuracy of thermal degradation measurements or the strong resistance of the polymers, poly(acrylic acid) and poly(allylamine hydrochloride), to NaCl. Such effects may also be responsible for the apparently weaker resistance to monovalent salt than the divalent case in ref. 48. On the other hand, the two divalent cases studied in ref. 48 gave similar results, although the salt-resistance seems marginally stronger for $SrCl_2$ than $CaCl_2$. Ultimately, the difference in polymer chemistry and measurement protocol prevents the quantitative comparison between their data and ours. However, the

ion valence strongly influences the coacervation behaviors in both cases.

Examining the coacervate branch of binodal curve more closely, we note that the initial response of the coacervate polymer concentration to salt addition is more pronounced for divalent ions. This is consistent with the reduced salt resistance for $MgCl_2$ and $CaCl_2$, and can be rationalized by considering ionic screening, as we will show in **Sec. 3.3**.

3.2 Polymer and salt partitioning with divalent ions

With dual dye-labeling and ICP-MS measurements, we can independently determine the concentrations of individual species in both the supernatant and coacervate phases. This enables an analysis of both polyelectrolyte overcharging within a single phase and small ion partitioning between the two phases as a function of salt concentration.

The degree of overcharging is often used to quantify the amount of small ions needed to neutralize polyelectrolytes in the coacervate, and can be defined as

$$\%\ \text{overcharging} = 100 \times \left(C_{\mathrm{a}}^{(\mathrm{coac})} / C_{\mathrm{c}}^{(\mathrm{coac})} - 1 \right), \tag{8}$$

where $C_{\mathrm{a}}^{(\mathrm{coac})}$ and $C_{\mathrm{c}}^{(\mathrm{coac})}$ are the concentrations of polyanion and polycation in the coacervate. The sign of overcharging indicates whether the system has an excess of polyanion (> 0) or polycation (< 0).

The overcharging data plotted against exogenous salt concentration C_{s} are shown in **Fig. 3a**. To facilitate comparison between different salts, the value of C_{s} has been scaled by the maximum salt concentration for which phase separation was observed, $C_{\mathrm{s,\,max}}$. We caution that the first data points for $CaCl_2$ and $MgCl_2$ are susceptible to experimental uncertainty.

Despite the scattering, it is clear that the behaviors of overcharging for all three systems are similar. The overcharging values are all negative, indicating a slight enrichment of polycations in the coacervate phase, and decrease with salt addition modestly.

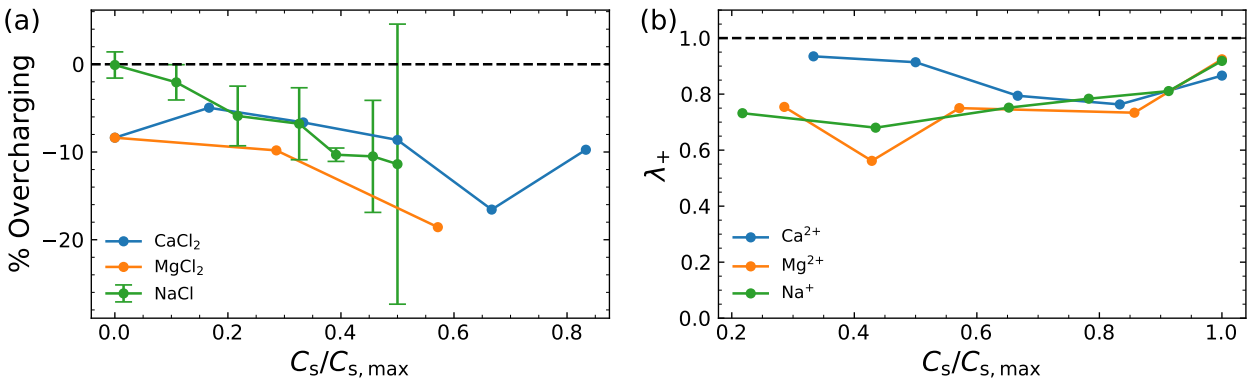

Figure 3: (a) Experimental overcharging and (b) salt partitioning measurements. Horizontal axis values correspond to bulk exogenous salt concentrations scaled by the largest concentration at which phase separation was observed for each salt, $C_{\mathrm{s,\,max}}$.

In samples containing NaCl, there is no obvious driving force to nonzero overcharging due to the symmetry of all charged species. In the divalent case, this symmetry is broken by the introduction of the divalent cation alongside monovalent anions. However, as discussed above, the data indicate that the choice of cation does not substantially affect the polyelectrolyte stoichiometry in the coacervate phase. So the degree of overcharging appears to be not correlated with ion valency. We speculate that the chemical specificity between the anion Cl^- and polyions used may be responsible for the observed sign of overcharging.

Using the cation concentrations determined from the ICP-MS measurements, we can compute the ion partition coefficients, defined as

$$\lambda_+ = C_+^{(\mathrm{coac})}/C_+^{(\mathrm{sup})}, \tag{9}$$

where $C_+^{(\mathrm{coac})}$ and $C_+^{(\mathrm{sup})}$ are the concentrations of small ions in coacervate and supernatant phases. The results are shown in **Fig. 3b**, against the scaled salt concentration. ICP-MS measurements for Cl^- ions are not accurate at these concentrations so are not included in our discussion.

For all three systems, the partition coefficients are below unity at nonzero added salt concentrations. Furthermore, regardless of salt, the values of λ_+ are smallest at intermedi-

ate salt concentrations before increasing toward unity as the salt concentration approaches $C_{\mathrm{s,\,max.}}$. As with the overcharging, there does not appear to be a significant dependence of the cation partitioning on the choice of salt.

The enrichment of small ions in the supernatant phase can be rationalized as follows. The supernatant is nearly devoid of polymers over the entire range of salt concentrations and thus the dissolution of more small ions in the supernatant than coacervate allows a large entropic gain at the cost of a relatively small loss of cohesive electrostatic interactions in the coacervate. As the bulk salt concentration approaches $C_{\mathrm{s,\,max.}}$, the polymer concentration becomes nearly equal in the two phases and the partition coefficient increases toward 1, as is seen.

As with the binodal curves, the data here can be compared with previous results. Previous works have experimentally investigated the partitioning of monovalent salts.[2,18,22,46–48] Generally, these experiments find a modest enrichment of ions in the supernatant phase for the majority of salt concentrations, consistent with our observation. However, some results[2,18] also indicate that monovalent ions are slightly enriched in the coacervate phase at low salt concentrations. Since the measurements adopted in these studies have varying degrees of precision, it is hard to draw a definitive conclusion.

On the other hand, various recent theoretical and computational efforts have attempted to explain this partitioning behavior.[2,22,55–59] While classical theories predict an ion-enriched coacervate phase,[23] these recent works are able to predict an ion-enriched supernatant in line with the majority of experimental observations. However, in all cases the predicted behavior and thus partitioning is sensitive to the details of the model, particularly to the treatment of excluded-volume interactions.[2]

The partitioning behavior observed here for both monovalent and divalent ions is similar to these early studies. However, given the sensitivity of theoretical predictions to model details, we speculate that the driving force for the enrichment of cations in the supernatant phase is chemically specific.

For divalent ions, experimental results are limited. In particular, the results from ref. 48 indicate an ion enriched supernatant phase in the presence of NaCl with partition coefficients slightly smaller than unity, as is the case here. For divalent salts $CaCl_2$ and $SrCl_2$, however, their measurements show that the coacervate is enriched in ions with partition coefficients as large as 10 in some cases. This result is in stark contrast to those seen here as well as theoretical predictions from ref. 45. The origin to this difference in partitioning behavior is difficult to discern based on the available data. As with the binodal curves, it is unclear whether the disagreement is a result of differences in the chemical specificity or measurement techniques. Accordingly we refrain from direct numerical comparison of partition coefficients and simply note that the effect of increasing cation valence in ref. 48 is qualitatively distinct from that observed here.

3.3 Analysis of valence effect in the low-salt regime

The effect of valence on the coacervate composition can be understood in terms of competition between mixing entropy and electrostatic correlation free energy. To illustrate this point, we analyze how the polymer concentration in the coacervate phase varies with the amount of salt added. In particular, we focus on the low-salt regime, where zero or little exogenous and endogenous salts are present.

In this regime, the contribution of the mixing entropy to the free energy, eq. (2), can be simplified considerably. The effects of the polyion molecular weight or degree of polymerization N on the coacervation behavior are weak; the molecular weight mainly changes the degree of salt resistance.[60] Thus, we consider the limiting case of infinitely long chains with $N \to \infty$, and drop the mixing entropy of polymer completely. The contribution of solvent entropy is treated with a virial expansion including two and three-body terms. Previous works[8,22] have shown that fitted values of $\chi \approx 1/2$ produce the best agreement between predicted and measured binodal concentrations for our system. The ideal solution condition of $\chi = 1/2$ is thus imposed and combined with the solvent entropy expansion to eliminate the

two-body term. The three-body coefficient w is left unspecified so that its effect is apparent analytically. With these simplifications, eq. (2) reduces to

$$f_{\mathrm{m}} = \phi_{\mathrm{s}} \ln \phi_{\mathrm{s}} + w\phi_{\mathrm{p}}^3, \tag{10}$$

where $\phi_{\mathrm{s}} = \phi_+ + \phi_-$ and $\phi_{\mathrm{p}} = \phi_{\mathrm{a}} + \phi_{\mathrm{c}}$ include contributions from both positive and negative small ions and polyelectrolytes. We stress that the polycation and polyanion are treated simultaneously because they are homologous.

The electrostatic correlation free energy can likewise be simplified. Eqation (4) is dominated by contributions from the intermediate-q range. Thus, the structure factor can be replaced with the Edwards approximation, $g(x) \simeq 2/x$. To further enable an analytical form, the standard approach of subtracting the diverging self-energy contribution is applied rather than the smearing approach described in **Sec. 2.3**. These simplifications have been adopted in previous works studying polyelectrolyte solution thermodynamics.[2,9,49,50] At this level of treatment, eq. (4) becomes

$$f_{\mathrm{e}} = 2\,p\,\phi_{\mathrm{p}}^{3/4}(1-s)\sqrt{2+s}, \tag{11}$$

where $p \equiv \frac{1}{3\pi}(3\pi l_{\mathrm{B}}\sigma^2/b^2)^{3/4}$, $s \equiv r z_+ z_- \phi_{\mathrm{s}}\phi_{\mathrm{p}}^{-1/2}$, and $r \equiv (\pi l_{\mathrm{B}} b^2/3\sigma^2)^{1/2}$. The parameters p and r depend essentially on charge density σ and chain stiffness b, whereas the parameter s depends on the ion and polymer concentration. Combining the above contribution with the mixing entropy, eqn. (10), the total free energy can be written as

$$f = \phi_{\mathrm{s}} \ln \phi_{\mathrm{s}} + w\phi_{\mathrm{p}}^3 + 2p\phi_{\mathrm{p}}^{3/4}(1-s)\sqrt{2+s}. \tag{12}$$

Equation (12) explicitly depends on the salt valence z_+ and z_-, and will be used to analyze the variation of coacervate composition with salt addition.

In the binary limit, i.e. $\phi_{\mathrm{s}} \to 0$, the supernatant is essentially depleted of polymer.

Consequently, the only species present in both phases is solvent, and the limiting value of polymer concentration ϕ_{p}^{*} is determined by balancing the chemical potential of solvent. Since the solvent composition is not explicitly included in our model, we use the osmotic pressure, $\Pi \equiv \sum_i \phi_i \, \partial f / \partial \phi_i - f$, as a surrogate for the solvent chemical potential. In this limit, the osmotic pressure for the supernatant phase vanishes, and that for for the coacervate phase is derived from eqn. (12). Equating the two values and setting $\phi_{\mathrm{s}} = 0$ gives ϕ_{p}^{*},

$$\phi_{\mathrm{p}}^{*} \simeq \left(\frac{l_{\mathrm{B}} \sigma^2}{4 b^2 w^{4/3} (3\pi)^{1/3}} \right)^{1/3} \propto l_{\mathrm{B}}^{1/3} \sigma^{2/3}, \tag{13}$$

which increases with the Bjerrum length, the charge density, but is independent of the ion valence. The effect of the cubic term is reflected by the dependence on w.

Upon addition of a small amount of salt, the ions partition into the supernatant and coacervate phases with concentrations $\phi_{\mathrm{s}}^{(\mathrm{sup})}$ and $\phi_{\mathrm{s}}^{(\mathrm{coac})}$. The result is a coacervate phase comprised of salt, polymer, and water in equilibrium with a dilute salt solution. In this case, all phases contain small ions and solvent. Phase compositions are thus determined by the equality of exchange chemical potentials for small ions, $\mu_{\mathrm{s}} \equiv \partial f / \partial \phi_{\mathrm{s}}$, as well as the osmotic pressure between the phases. As with Π, an expression for μ_{s} is computed from eq. (12). The values of μ_{s} are equated between the two phases and the resulting equation is rearranged to yield the ratio of total small ion concentrations in the two phases (SI, eq. (S.24)),

$$\ln \left(\frac{\phi_{\mathrm{s}}^{(\mathrm{coac})}}{\phi_{\mathrm{s}}^{(\mathrm{sup})}} \right) \simeq \mu_{\mathrm{s,coac}}^{(\mathrm{el})} \left(\phi_{\mathrm{p}}^{(\mathrm{coac})} \right). \tag{14}$$

Here, $\phi_{\mathrm{p}}^{(\mathrm{coac})}$ is the coacervate polymer concentration after salt addition. The left side of eq. (14) results from the translational entropy of small ions in both phases. The right-hand side is the excess exchange chemical potential for small ions, $\mu_{\mathrm{s,coac}}^{(\mathrm{el})}$, which depends only on the polymer concentration in the coacervate phase. The subscript "coac" and superscript "el" denote a potential resulting from favorable electrostatic correlations between polyelectrolytes

and small ions in the coacervate phase. In this analysis, the coacervate polymer concentration is constrained to within a small deviation from that in the zero-salt limit, $\phi_{\mathrm{p}} = \phi_{\mathrm{p}}^{*}(1 + \delta\phi_{\mathrm{p}})$ with $\delta\phi_{\mathrm{p}} \to 0$.

With the relative amounts of salt in each phase specified by the small ion chemical potential balance, the polymer concentration in the coacervate is determined by equating the osmotic pressures. Leveraging the result of eqn. (14), the variation of polymer concentration $\delta\phi_{\mathrm{p}}$ can be expressed as (SI)

$$\delta\phi_{\mathrm{p}} \simeq -z_{+}z_{-}c\left[1 - \frac{\mu_{\mathrm{s,coac}}^{(\mathrm{el})}\left(\phi_{\mathrm{p}}^{*}\right)}{3}\right]\phi_{\mathrm{s}}^{(\mathrm{sup})} \tag{15}$$

where $c = \left(2\pi^{5/3} l_{\mathrm{B}} b^{4} w^{2/3} / 3^{4/3}\sigma^{4}\right)^{1/3}$. The above scaling results from the competition between electrostatic correlations in the coacervate phase, translational entropy of small ions, and polymer-solvent interactions (the cubic term). The explicit dependence on ion valence derives from the electrostatic correlation free energy and can be attributed to the screening effects.

When salts are added to the system, the dissolved ions are distributed between the coexisting phases, increasing their osmotic pressure. In the coacervate phase, the newly added salts screen out favorable electrostatic interactions between polyelectrolyte chains, causing the osmotic pressure to be higher than the supernatant phase. To compensate for this effect, the coacervate phase must swell by taking more water, effectively decreasing the polymer content, as is seen here. This screening effect is dependent on the strength of electrostatic interactions and is thus a function of the ion valence, as shown in eq. (15). The decrease of polymer concentration in the coacervate phase upon salt addition is more pronounced for systems with multivalent small ions, roughly in proportion to the product $z_{+}z_{-}$. Such dependence in the limit $\phi_{\mathrm{s}} \to 0$ is sketched in **Fig. 4a**, for $z_{+} = 1$, 2, and 3, showing clearly how the limiting slope $\partial\phi_{\mathrm{s}}/\partial\phi_{\mathrm{p}}$ is reduced as valence is increased.

The dependence on $z_{+}z_{-}$ in eq. (15) can be understood by considering charge neutrality.

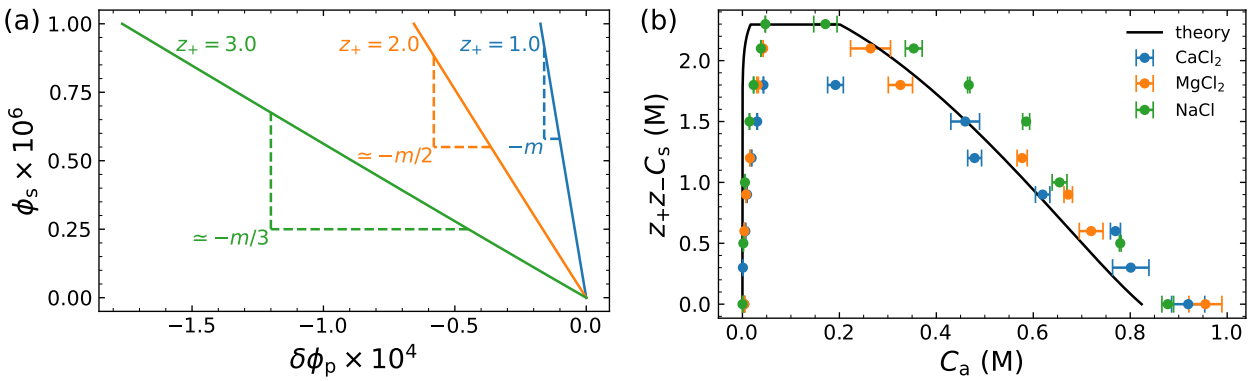

Figure 4: (a) Predicted response of coacervate polymer concentration to the addition of salts with cation valence z_+ and (b) Scaled binodal curves for the polyanion concentration. Vertical axis values have been multiplied by the corresponding small ion valences. Note the overlap of the coacervate branches in the low-salt regime. The solid black line is the binodal envelope predicted by an analogous theory to that outlined in **Sec. 2.3**, which has been employed in previous works.[8,11,14,22]

Charge neutrality implies that the number of small cations and anions in the bulk are related by $n_+z_+ = n_-z_-$, which leads to $C_\pm = C_s z_\mp/(z_+ + z_-)$. It follows that the ionic strength, $z_+^2 C_+ + z_-^2 C_-$, can be written as $z_+z_-C_s$.

The above analysis motivates the visualization of the binodal curves in terms of the product $z_+z_-C_s$, as shown in **Fig. 4b**. It is remarkable that the binodal concentrations for all three types of salts nearly overlap in the low-salt regime, lending strong support to the above asymptotic analysis. At higher values of C_s, a subtle but clear pattern emerges in the stability of the coacervate phase to different cations at the same ionic strength. Fortuitously, these same three salts were investigated in the past.[41] Comparing the turbidity at high ionic strengths, their data indicate the same ordering of cation stability, $Na^+ > Mg^{2+} > Ca^{2+}$; the ordering also agrees with the well-known Hofmeister series.[41–44] Previous works have discussed this effect in terms of differing solvation environments between various ions and surrounding solvent moecules,[6] hinting at the potential impact of solvent ordering on phase behavior. More work is needed to fully explore this area.[16,53] Our data, although preliminary, shows that the Hofmeister effect is much weaker than the effect of ion valence.

The solid black line in **Fig. 4b** is the theoretical prediction for the binodal concentra-

tion of solutions containing monovalent salts, computed using an analogous model to that outlined in **Sec. 2.3** according to the procedure outlined in previous works.[8,11,14,22] This approach incorporates reversible ion binding[10,11] but does not account for ion valence and is thus only directly applicable to monovalent ions. The agreement between the predicted and measured values is nearly quantitative over the full range of measured ionic-strengths. Notably, the upper maximum salt concentration is overestimated for $CaCl_2$ and $MgCl_2$. This is not unexpected as the treatment of reversible ion binding for divalent ions is more complicated than the monovalent ions because both inter- and intra-molecular binding require consideration. We leave the discussion of such valence effects to future work.

4 Conclusions

In summary, solutions of homologous polyelectrolytes were used to investigate the effects of salt valence on coacervation behavior. The binodal diagrams were compared between monovalent salt and two types of divalent salts. The concentrations of polyanions, polycations, and cations in both the coacervate and supernatant phases were determined using UV-Vis absorbance and ICP-MS measurements. Both binodal diagrams and the partitioning behaviors of small ions and polyions are compared to reveal the effects of valence. We found that the binodal diagrams show a much weaker salt resistance as valence is increased, in agreement with earlier experimental work based on turbidity measurements[41] and a recent theoretical study.[45]

Analysis of the small ion partitioning showed that the supernatant phase was enriched in small ions at all nonzero salt concentrations. This is consistent with the majority of experimental results from past literature studies.[2] In contrast, however, the results of ref. 48 indicate an ion-enriched coacervate phase. We speculate that the ion partitioning behavior is less universal than the generic shape of the binodal curve and depends sensitively on the chemical-specific interactions. Furthermore, analysis of the polycation and polyanion

concentrations showed that the coacervate phase is slightly enriched in polycations regardless of salt concentration, which we again suspect is a specific feature of our system.

The valence-dependence of binodal curves is analysed using the model we developed recently,[8,11,22] which treats the electrostatic correlations using the RPA. Focusing on the low-salt regime, we showed that the effects of valence can be understood as a result of enhanced screening, and examined how polymer concentration varies with the addition of salts. The explicit dependence on ion valence allows us to collapse the binodal diagrams from both monovalent and divalent ions, by scaling the ion concentration with the product z_+z_-.

Our work is limited to A_2B types of salts. The collapse of data by considering ionic screening encourages the expanded study with other types of multivalence, in particular AB_2 and A_2B_2 type salts. Higher-valence (e.g. trivalent salts) should be explored as well. Although the observations made here may not be readily extrapolated, given the complexity of precipitation behavior revealed in the earlier work,[30,32,37–40] we anticipate that the richer coacervation behaviors to be identified will better inform the theoretical modeling of valence effects.

Acknowledgement

This research was partially supported by the National Science Foundation CAREER Award through DMR-1846547. J.Q. acknowledges support from Stanford University Terman Faculty Fellowship. J.H. acknowledges support from the Stanford Bio-X Bowes Graduate Student Fellowship.

Supporting Information Available

Experimental calibration curves, additional phase diagrams, and derivation of results in **Sec. 3.3** (PDF)

References

(1) Srivastava, S.; Tirrell, M. V. *Advances in Chemical Physics*; John Wiley & Sons, Ltd, 2016.

(2) Sing, C. E.; Perry, S. L. Recent progress in the science of complex coacervation. *Soft Matter* **2020**, *16*, 2885–2914.

(3) Rumyantsev, A. M.; Jackson, N. E.; de Pablo, J. J. Polyelectrolyte complex coacervates: Recent developments and new frontiers. *Annual Review of Condensed Matter Physics* **2021**, *12*, 155–176.

(4) Banani, S. F.; Lee, H. O.; Hyman, A. A.; Rosen, M. K. Biomolecular condensates: organizers of cellular biochemistry. *Nature Reviews Molecular Cell Biology* **2017**, *18*, 285–298.

(5) Boeynaems, S.; Alberti, S.; Fawzi, N. L.; Mittag, T.; Polymenidou, M.; Rousseau, F.; Schymkowitz, J.; Shorter, J.; Wolozin, B.; Van Den Bosch, L.; Tompa, P.; Fuxreiter, M. Protein phase separation: A new phase in cell biology. *Trends in Cell Biology* **2018**, *28*, 420–435.

(6) Ghasemi, M.; Larson, R. G. Future directions in physiochemical modeling of the thermodynamics of polyelectrolyte coacervates. *AIChE Journal* **2022**, *68*, e17646.

(7) Muthukumar, M. 50th anniversary perspective: A perspective on polyelectrolyte solutions. *Macromolecules* **2017**, *50*, 9528–9560.

(8) Lou, J.; Friedowitz, S.; Qin, J.; Xia, Y. Tunable coacervation of well-defined homologous polyanions and polycations by local polarity. *ACS Central Science* **2019**, *5*, 549–557.

(9) Qin, J.; de Pablo, J. J. Criticality and connectivity in macromolecular charge complexation. *Macromolecules* **2016**, *49*, 8789–8800.

(10) Salehi, A.; Larson, R. G. A molecular thermodynamic model of complexation in mixtures of oppositely charged polyelectrolytes with explicit account of charge association/dissociation. *Macromolecules* **2016**, *49*, 9706–9719.

(11) Friedowitz, S.; Salehi, A.; Larson, R. G.; Qin, J. Role of electrostatic correlations in polyelectrolyte charge association. *The Journal of Chemical Physics* **2018**, *149*, 163335.

(12) Chang, L.-W.; Lytle, T. K.; Radhakrishna, M.; Madinya, J. J.; Vélez, J.; Sing, C. E.; Perry, S. L. Sequence and entropy-based control of complex coacervates. *Nature Communications* **2017**, *8*, 1273.

(13) Shen, K.; Wang, Z.-G. Electrostatic correlations and the polyelectrolyte self energy. *The Journal of Chemical Physics* **2017**, *146*, 084901.

(14) Friedowitz, S.; Qin, J. Reversible ion binding for polyelectrolytes with adaptive conformations. *AIChE Journal* **2021**, *67*, e17426.

(15) Zhang, P.; Wang, Z.-G. Supernatant phase in polyelectrolyte complex coacervation: Cluster formation, binodal, and nucleation. *Macromolecules* **2022**, *55*.

(16) Chen, S.; Wang, Z.-G. Driving force and pathway in polyelectrolyte complex coacervation. *Proceedings of the National Academy of Sciences* **2022**, *119*.

(17) Spruijt, E.; Westphal, A. H.; Borst, J. W.; Cohen Stuart, M. A.; van der Gucht, J. Binodal compositions of polyelectrolyte complexes. *Macromolecules* **2010**, *43*.

(18) Li, L.; Srivastava, S.; Andreev, M.; Marciel, A. B.; de Pablo, J. J.; Tirrell, M. V. Phase behavior and salt partitioning in polyelectrolyte complex coacervates. *Macromolecules* **2018**, *51*.

(19) Li, L.; Rumyantsev, A. M.; Srivastava, S.; Meng, S.; de Pablo, J. J.; Tirrell, M. V. Effect of solvent quality on the phase behavior of polyelectrolyte complexes. *Macromolecules* **2021**, *54*, 105–114.

(20) Ali, S.; Bleuel, M.; Prabhu, V. M. Lower critical solution temperature in polyelectrolyte complex coacervates. *ACS Macro Letters* **2019**, *8*.

(21) Adhikari, S.; Prabhu, V. M.; Muthukumar, M. Lower critical solution temperature behavior in polyelectrolyte complex coacervates. *Macromolecules* **2019**, *52*.

(22) Friedowitz, S.; Lou, J.; Barker, K. P.; Will, K.; Xia, Y.; Qin, J. Looping-in complexation and ion partitioning in nonstoichiometric polyelectrolyte mixtures. *Science Advances* **2021**, *7*.

(23) Overbeek, J. T. G.; Voorn, M. J. Phase separation in polyelectrolyte solutions. theory of complex coacervation. *Journal of Cellular and Comparative Physiology* **1957**, *49*, 7–26.

(24) Bloomfield, V. A. DNA condensation by multivalent cations. *Biopolymers* **1997**, *44*, 269–282.

(25) Raspaud, E.; Olvera de la Cruz, M.; Sikorav, J. L.; Livolant, F. Precipitation of DNA by polyamines: A polyelectrolyte behavior. *Biophysical Journal* **1998**, *74*, 381–393.

(26) Yang, M.; Digby, Z. A.; Chen, Y.; Schlenoff, J. B. Valence-induced jumps in coacervate properties. *Science Advances* **2022**, *8*, eabm4783.

(27) Ermoshkin, A. V.; Olvera de la Cruz, M. Polyelectrolytes in the presence of multivalent ions: Gelation versus segregation. *Physical Review Letters* **2003**, *90*, 125504.

(28) Babinchak, W. M.; Surewicz, W. K. Liquid–Liquid Phase Separation and Its Mechanistic Role in Pathological Protein Aggregation. *Journal of Molecular Biology* **2020**, *432*, 1910–1925.

(29) de la Cruz, M. O.; Belloni, L.; Delsanti, M.; Dalbiez, J. P.; Spalla, O.; Drifford, M. Precipitation of highly charged polyelectrolyte solutions in the presence of multivalent salts. *The Journal of Chemical Physics* **1995**, *103*, 5781–5791.

(30) Sabbagh, I.; Delsanti, M. Solubility of highly charged anionic polyelectrolytes in presence of multivalent cations: Specific interaction effect. *The European Physical Journal E* **2000**, *1*, 75–86.

(31) Hsiao, P.-Y.; Luijten, E. Salt-induced collapse and reexpansion of highly charged flexible polyelectrolytes. *Physical Review Letters* **2006**, *97*, 148301.

(32) Hansch, M.; Hämisch, B.; Schweins, R.; Prévost, S.; Huber, K. Liquid-liquid phase separation in dilute solutions of poly(styrene sulfonate) with multivalent cations: Phase diagrams, chain morphology, and impact of temperature. *The Journal of Chemical Physics* **2018**, *148*, 014901.

(33) Jacobs, M.; Lopez, C. G.; Dobrynin, A. V. Quantifying the effect of multivalent ions in polyelectrolyte solutions. *Macromolecules* **2021**, *54*, 9577–9586.

(34) Wittmer, J.; Johner, A.; Joanny, J. F. Precipitation of polyelectrolytes in the presence of multivalent salts. *Journal de Physique II* **1995**, *5*, 635–654.

(35) Solis, F. J.; de la Cruz, M. O. Collapse of flexible polyelectrolytes in multivalent salt solutions. *The Journal of Chemical Physics* **2000**, *112*, 2030–2035.

(36) Lee, C.-L.; Muthukumar, M. Phase behavior of polyelectrolyte solutions with salt. *The Journal of Chemical Physics* **2009**, *130*, 024904.

(37) Narh, K. A.; Keller, A. Precipitation effects in polyelectrolytes on addition of salts. *Journal of Polymer Science Part B: Polymer Physics* **1993**, *31*, 231–234.

(38) Prabhu, V. M.; Muthukumar, M.; Wignall, G. D.; Melnichenko, Y. B. Dimensions of polyelectrolyte chains and concentration fluctuations in semidilute solutions of sodium–poly(styrene sulfonate) as measured by small-angle neutron scattering. *Polymer* **2001**, *42*, 8935–8946.

(39) Prabhu, V. M.; Muthukumar, M.; Wignall, G. D.; Melnichenko, Y. B. Polyelectrolyte chain dimensions and concentration fluctuations near phase boundaries. *The Journal of Chemical Physics* **2003**, *119*.

(40) Delsanti, M.; Dalbiez, J. P.; Spalla, O.; Belloni, L.; Drifford, M. *Macro-ion Characterization*; ACS Symposium Series 548; American Chemical Society, 1993; Vol. 548; pp 381–392.

(41) Perry, S. L.; Li, Y.; Priftis, D.; Leon, L.; Tirrell, M. The effect of salt on the complex coacervation of vinyl polyelectrolytes. *Polymers* **2014**, *6*, 1756–1772.

(42) Hofmeister, F. Zur lehre von der wirkung der salze. *Archiv für experimentelle Pathologie und Pharmakologie* **1888**, *24*, 247–260.

(43) Kunz, W.; Henle, J.; Ninham, B. W. 'Zur Lehre von der Wirkung der Salze' (about the science of the effect of salts): Franz Hofmeister's historical papers. *Current Opinion in Colloid & Interface Science* **2004**, *9*, 19–37.

(44) Kunz, W.; Lo Nostro, P.; Ninham, B. W. The present state of affairs with Hofmeister effects. *Current Opinion in Colloid & Interface Science* **2004**, *9*, 1–18.

(45) Lytle, T. K.; Sing, C. E. Tuning chain interaction entropy in complex coacervation using polymer stiffness, architecture, and salt valency. *Molecular Systems Design & Engineering* **2018**, *3*, 183–196.

(46) Liu, Y.; Momani, B.; Henning Winter, H.; L. Perry, S. Rheological characterization of liquid-to-solid transitions in bulk polyelectrolyte complexes. *Soft Matter* **2017**, *13*.

(47) Radhakrishna, M.; Basu, K.; Liu, Y.; Shamsi, R.; Perry, S. L.; Sing, C. E. Molecular connectivity and correlation effects on polymer coacervation. *Macromolecules* **2017**, *50*.

(48) Iyer, D.; Syed, V. M. S.; Srivastava, S. Influence of divalent ions on composition and viscoelasticity of polyelectrolyte complexes. *Journal of Polymer Science* **2021**, *59*, 2895–2904.

(49) Borue, V. Y.; Erukhimovich, I. Y. A statistical theory of weakly charged polyelectrolytes: fluctuations, equation of state and microphase separation. *Macromolecules* **1988**, *21*.

(50) Borue, V. Y.; Erukhimovich, I. Y. A statistical theory of globular polyelectrolyte complexes. *Macromolecules* **1990**, *23*.

(51) Israelachvili, J. N. *Intermolecular and Surface Forces*; Academic Press, 2010.

(52) Braus, M. The theory of electrolytes. i. freezing point depression and related phenomena (translation). **2019**,

(53) Beckinghausen, M.; Spakowitz, A. J. Interplay of polymer structure, solvent ordering, and charge fluctuations in polyelectrolyte solution thermodynamics. *Macromolecules* **2023**, *56*.

(54) Chen, S.; Zhang, P.; Wang, Z.-G. Complexation between oppositely charged polyelectrolytes in dilute solution: Effects of charge asymmetry. *Macromolecules* **2022**, *55*.

(55) Zhang, P.; Alsaifi, N. M.; Wu, J.; Wang, Z.-G. Polyelectrolyte complex coacervation: Effects of concentration asymmetry. *The Journal of Chemical Physics* **2018**, *149*.

(56) Perry, S. L.; Sing, C. E. PRISM-based theory of complex coacervation: Excluded volume versus chain correlation. *Macromolecules* **2015**, *48*.

(57) Adhikari, S.; Leaf, M. A.; Muthukumar, M. Polyelectrolyte complex coacervation by electrostatic dipolar interactions. *The Journal of Chemical Physics* **2018**, *149*.

(58) Kudlay, A.; Olvera de la Cruz, M. Precipitation of oppositely charged polyelectrolytes in salt solutions. *The Journal of Chemical Physics* **2004**, *120*.

(59) Kudlay, A.; Ermoshkin, A. V.; Olvera de la Cruz, M. Complexation of oppositely charged polyelectrolytes: Effect of ion pair formation. *Macromolecules* **2004**, *37*.

(60) Qin, J.; Priftis, D.; Farina, R.; Perry, S. L.; Leon, L.; Whitmer, J.; Hoffmann, K.; Tirrell, M.; de Pablo, J. J. Interfacial tension of polyelectrolyte complex coacervate phases. *ACS Macro Letters* **2014**, *3*.